J Appl Electrochem (2013) 43:467–479
DOI 10.1007/s10800-013-0531-8

ORIGINAL PAPER

Photoelectrocatalytic bleaching of *p*-nitrosodimethylaniline using Ti/TiO_2 nanostructured electrodes deposited by means of a pulsed laser deposition process

Rimeh Daghrir · Patrick Drogui · Ibrahima Ka · My Ali El Khakani · Didier Robert

Received: 20 October 2012 / Accepted: 24 January 2013 / Published online: 6 February 2013

Abstract This study investigated the potential use of oxidation in a photoelectrocatalytic cell for bleaching *p*-nitrosodimethylaniline. The Ti/TiO_2 used as photo-anode was prepared by a pulsed laser deposition method. The TiO_2 coatings were found to have rutile and anatase structures consisting of approximately 10 and 15 nm in diameter, respectively. A relatively high degradation rate of *p*-nitrosodimethylaniline was recorded using the photoelectrocatalytic cell, compared to those measured during conventional electrochemical oxidation, direct photolysis and photocatalysis processes. The influence of different parameters such as crystallographic structure of Ti/TiO_2, type of cathode, potential applied, electrolysis time, UV irradiation and initial pH were investigated. The photoelectrocatalytic cell using Ti/TiO_2 (anatase structure) as photo-anode and vitreous carbon as cathode operated at a current intensity of 0.1 A for 120 min with 254 nm of UV irradiation was found to have the best conditions to remove high amounts of *p*-nitrosodimethylaniline (22.6×10^{-3} mM h^{-1}).

Keywords Photoelectrocatalytic oxidation · *p*-Nitrosodimethylaniline · Reactive oxygen species · Titanium dioxide semiconductor photocatalyst

List of symbols

CB	Conduction band
DP	Direct photolysis
EO	Electro-oxidation
Gr	Graphite
PC	Photocatalysis
PECO	Photoelectrocatalytic oxidation
PLD	Pulsed laser deposition
RNO	*p*-Nitrosodimethylaniline
ROS	Reactive oxygen species
SS	Stainless steel
SEM	Scanning electron microscopy
TiO_2	Titanium dioxide
VB	Valence band
VC	Vitreous carbon
XRD	X-ray diffraction
XPS	X-ray photoelectron spectroscopy

1 Introduction

Photo-oxidation, using semiconductors as photocatalysts, has been widely applied over the last ten years for removing organic pollutants [1–3]. These techniques are capable of destroying undesirable organic compounds (such as herbicides, pesticides, dyes, detergents and phenol

R. Daghrir · P. Drogui (✉)
Institut national de la recherche scientifique, Centre Eau, Terre et Environnement, Université du Québec, 490 rue de la Couronne, Québec, QC G1K 9A9, Canada
e-mail: patrick.drogui@ete.inrs.ca

R. Daghrir
e-mail: rimeh.daghrir@ete.inrs.ca

I. Ka · M. A. El Khakani
Institut national de la recherche scientifique, INRS-Énergie, Matériaux et Télécommunications, Université du Québec, 1650, Blvd. Lionel-Boulet, Varennes, QC J3X 1S2, Canada
e-mail: Ka@emt.inrs.ca

M. A. El Khakani
e-mail: elkhakani@emt.inrs.ca

D. Robert
Antenne de Saint-Avold du Laboratoire des Matériaux, Surface et Procédés pour la Catalyse (LMSPC) CNRS-UMR 7515, Université De Lorraine, 12 rue Victor Demange, 57500 Saint-Avold, France
e-mail: didier.robert@univ-lorraine.fr

compounds) in aqueous media and removing traces of organic species that are stable and difficult to oxidise by means of conventional water treatment methods [4–7]. Nowadays, photocatalytic process using semiconductor as photocatalyst (ex. TiO_2) under UV irradiation has been extensively applied for the oxidation of various refractory organic compounds such as bisphenol A, tetracycline, sulfamethazine etc. [8–10]. The basic mechanism of photocatalysis (PC) involves ejecting an electron from the valence band (VB) to the conduction band (CB) of the titanium dioxide (TiO_2) semiconductor, thereby creating an 'h^+' hole in the VB (Eq. 1). The delocalization of electrons occurs during UV irradiation of TiO_2 with energy equal to or greater than the band gap (>3.2 eV). These charge carriers (e^-/h^+) can migrate to the surface of the catalyst, where they are then available to undergo redox reactions with substrates [5]. Nonetheless, the fast recombination of the photogenerated electron/hole (e^-/h^+) reduces the photonic efficiency and represents the major drawback of PC applications [11, 12]. According to Meng et al. [13], the PC efficiency of a semiconductor depends on three physical processes, including the light absorption, the transport of charge carriers and the recombination of photogenerated electron–hole pairs.

$$TiO_2 + h\upsilon \rightarrow e^-_{CB} + h^+_{VB} \quad (1)$$

Recently, scientists have explored methods to chemically modify the photo-catalyst. An impurity doping the photo-catalyst (either cations or anions) is one of the typical approaches that has been applied by several research works to enhance the photocatalytic activity towards the organic compounds such as the methyl orange [13, 14]. Another approach using for example ZnO photocatalyst coupled to another semi-conductor (CeO_2) has been conducted by Ma et al. [15] to ensure higher photocatalytic performance for the degradation of rhodamine B. These new photo-catalyst materials ensure to extend the response towards the visible light and prevent the fast recombination of excited electron/holes during photocatalytic process [13, 15]. Despite the several advantages achieved by doping photo-catalyst with cations or anions, some researchers have found that the content of dopant would decrease during the annealing process, thus reducing the photocatalytic activity [16]. As reported in previous research [17], the metal doped material have been shown to suffer from thermal instability and metals centres act as electron traps which encourage the recombination of the e^-/h^+ pairs.

By comparison, photoelectrocatalytic treatment has received considerable attention in the environmental field owing to its ability to retard the recombination of electron–hole pairs (e^-_{CB}/h^+_{VB}) and the possibility to increase the lifetime of the electron–hole pairs. The photoelectrocatalytic technique combines both electrolytic and photocatalytic processes [18]. The applied external potential is a key factor in the process because it accelerates the PC reaction [11, 18–20]. The applied external potential prevents the recombination between the photogenerated electrons and holes. Photogenerated electrons in the excited TiO_2 anode can be removed via an external bias, instead of electron transfer to molecular oxygen. As reported by Fujishima et al. [21], the photogenerated electrons (e^-) increase the TiO_2 conductivity and enhance the photocatalytic activity. However, the recombination between e^-/h^+ pairs reduces the quantum efficiency [22]. Every recombination means a loss of a hole, a reduction in the TiO_2 conductivity and thus a decrease in the photoelectrocatalytic reaction. The external potential applied in photoelectrocatalytic process avoids their recombination by ejecting the electrons in the CB. Consequently, a photogenerated hole, or OH°, is left at the surface of the TiO_2 electrode. In the VB of the TiO_2 photocatalyst, the holes can react with adsorbed water to form hydroxyl radicals (OH°) [Eq. (2)], whereas in the CB of TiO_2, the excited electrons are trapped by O_2 to form the superoxide radical ion (O_2^-) [Eq. (3)] [23].

$$h^+_{vb} + OH^- \rightarrow HO^{\circ}_{ads} \quad (2)$$

$$e^-_{CB} + O_2 \rightarrow O_2^{o-} \quad (3)$$

Other reactive oxygen species (e.g. O_3, H_2O_2 etc.) can be formed during photo-electro-catalysis [24–26]. The addition of an electron acceptor to the system, such as hydrogen peroxide and ozone, prevents the electron–hole recombination and increases the photocatalyst efficiency [24]. Among these reactive oxygen species (ROS), hydroxyl radical is by far one of the most powerful oxidants that can be used in water treatment. It is highly reactive and characterised by a half-life of approximately 10^{-9} s [3, 27]. However, the short lifetime and the high reactivity of the hydroxyl radical make its detection very difficult. Methods for detecting hydroxyl radicals include electron paramagnetic resonance (EPR) spectroscopy [28], fluorometric assay [29] and high performance liquid chromatography [30]. Nevertheless, the application of these methods is very difficult due to the need for expensive reagents and complex operation procedures [2]. UV–Visible absorption spectroscopy method is applied to investigate the hydroxyl radical [2, 3, 23, 31, 32]. *p*-Nitrosodimethylaniline (RNO) is an organic dye molecule having a strong yellow colour in aqueous solution and is easy to detect using UV–Visible absorption spectroscopy (440 nm) [33]. RNO is bleached selectively by oxidation with hydroxyl radicals and does not react with singlet oxygen ($^1O_2$), superoxide anions (O_2^-) or other peroxy compounds [23, 33]. However, ozone, hypochlorous acid and hypochlorite are other strong chemical oxidants that have also been shown to bleach RNO by chemical oxidation [23].

The aim of this study is to evaluate the oxidation potential of a photoelectrocatalytic cell with a nanocrystalline TiO_2 photo-anode under UV irradiation [photoelectrocatalytic oxidation process (PECO)]. RNO was used as a probe molecule to assess the production of reactive oxygen species. Different parameters such as current intensity, crystallographic structure of the deposited TiO_2 films, UV irradiation, initial pH and the effect of ozone and hydrogen peroxide produced in situ were investigated.

2 Materials and methods

2.1 Ti/TiO_2 electrode preparation

TiO_2 coatings were prepared using a pulsed laser deposition (PLD) method. A KrF excimer laser (wavelength = 248 nm, pulse durations 15 ns) operating at a repetition rate of 30 Hz was focused, at an incidence angle of 45°, onto the TiO_2 rotating target (99.95 % purity). The on-target laser energy density was set to 4.5 J cm^{-2}. The TiO_2 films were deposited on both titanium grids (for photoelectrochemical studies) and on silicon substrates (for material characterisations). The TiO_2 films were deposited at a temperature of 600 and 400 °C, respectively, under an oxygen background pressure of 1 mTorr. The PLD deposition chamber was first turbo-pumped to approximately 10^{-6} Torr before filling it with oxygen. More details on the pulsed laser deposition system and it schematics can be found elsewhere [34]. Prior to coating the substrates, the TiO_2 target was systematically cleaned by laser-ablating its surface for 5 min. The nominal thickness of the coating was estimated to be 400 nm for rutile TiO_2 and 1.0 μm for anatase TiO_2. The film thickness was determined directly from cross-sectional scanning electron microscopy (SEM) observations. The crystallographic structure of the PLD-deposited TiO_2 films was examined by means of X-ray diffraction (XRD) using a Philips X'pert-MPD X-ray diffractometer (Cu-K_α radiation) at a glancing incident angle of 1°. The composition and chemical bonding states of the TiO_2 films were investigated by means of X-ray photoelectron spectroscopy (XPS) using Al K_a monochromatic radiation (1,487 eV) in an ESCALAB 200I-XL spectrophotometer after a systematic in situ surface cleaning by 5 keV Ar+ ion sputtering.

2.2 Preparation of the synthetic solution

RNO (*N*,*N*-dimethyl-4-nitroso-aniline) was an analytical grade reagent supplied by Sigma Aldrich (purity 97 %). An RNO stock solution (4×10^{-3} mol L^{-1}) was prepared in a glass tank containing 1 L of buffer in which 600.72 mg of RNO was added. Solubilisation of RNO was carried out by stirring at a speed of 900 rpm for 120 min. Mixing was achieved using a Teflon-covered stirring bar deposited in the bottom of the beaker. The RNO stock solution is stable for periods up to several weeks when protected from light. At the end of this conditioning stage, a fraction of the mixture (12 mL) was transferred into a 2 L tank containing 1 L of buffer solution. The resulting mixture constituted the synthetic RNO solution (final concentration of 4.80×10^{-5} mol L^{-1}) in which 0.05 mol L^{-1} of sodium sulphate was added to increase the electrical conductivity. Buffer solutions were prepared using anhydrous dibasic sodium phosphate (99 % purity) and crystalline monobasic potassium phosphate (99 % purity). The pH value of the buffer solution was 7.0.

2.3 Experimental device

The reactor unit was made of an acrylic material with dimensions of 12.7 cm (width), 16.51 cm (length) and 11.43 cm (depth). A quartz window (8.89×8.89 cm) was disposed on one face of the reactor for the photoelectrocatalysis experiments (Fig. 1). All of the assays were conducted in batch mode. The photoelectrocatalytic cell was composed of one anode (Ti/TiO_2) and one cathode, each having a surface area of 110 cm^2 (10 cm width × 11 cm high), placed in parallel and submerged in the solution. Different cathode materials were investigated: stainless steel (SS), vitreous carbon (VC) and graphite (Gr). The electrodes were installed vertically on a perforated Plexiglas plate placed 2 cm from the bottom of the cell. The inter-electrode gap was 1.0 cm. Both the anode and cathode were connected to the positive and negative outlets, respectively, of a regulated DC power supply (PS 3030 D, Circuit-Test Electronics, Burnaby, BC, Canada) with a maximum current rating of 3.0 A at an open circuit potential of 30 V. The photoelectrocatalytic cell was operated at currents ranging from 0.02 to 0.1 A for treatment periods of 120 min. Two mercury lamps with 254 nm

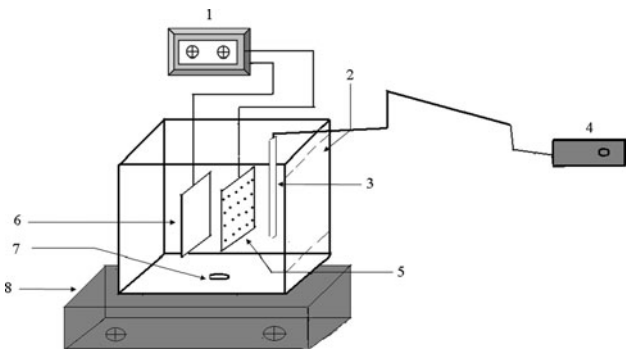

Fig. 1 Schematic diagram of the photoelectrocatalytic reactor *1* DC power supply, *2* quartz window, *3* UV lamp, *4* photometer, *5* photoanode, *6* cathode, *7* stirring bar and *8* magnetic stirrer

(light intensity = 6.9 mW cm^{-2}) and 365 nm (light intensity = 0.3 mW cm^{-2}) illumination were used to irradiate the catalytic surface of Ti/TiO_2 photo-anode. The lamp was positioned vertically on a support inside the reactor. The light intensity was measured with a photometer (Model PS-3, 99-0057-01; UVP Company, USA). The light intensity is the luminous power imposed per unit area of photoelectrocatalytic reactor. The photoelectrocatalytic reactor was placed in a dark chamber to avoid interference from the daylight. Mixing in the cell was achieved using a Teflon-covered stirring bar installed between the perforated plate and the bottom of the cell. All experiments were carried out at room temperature (25 °C). For all tests a total volume of 1.0 L was used. Na_2SO_4 (0.05 M) was used as the supporting electrolyte. For the reactions at different pH, hydrochloric acid or sodium hydroxide solutions were added to adjust the initial pH of the RNO solution. Sodium sulphate was an analytical grade reagent supplied by Mat laboratory (Quebec, QC, Canada). Anhydrous dibasic sodium phosphate and crystalline monobasic potassium phosphate were analytical grade reagents and supplied by EMD Chemicals (Darmstadt, Germany).

2.4 Analytical techniques

The pH was determined using a pH meter (Fisher Acumet model 915) equipped with a double-junction Cole-Palmer electrode with an Ag/AgCl reference cell. The bleaching rate was monitored by absorbance measurements of RNO at 440 nm using an UV–Visible absorption spectrophotometer (UV 0811 M136, Varian, Australia). The RNO calibration curve was obtained by plotting the RNO absorbance at 440 nm as a function of RNO concentration (from 0.0 to 5.32×10^{-5} mol L^{-1}). ROS (O_3 and OH°) produced in situ have been shown to bleach RNO by chemical oxidation [12]. The oxidising species include the "h^+" holes created in the VB.

The hydrogen peroxide concentration was measured using volumetric dosage. The cerium ion solution [$Ce(SO_4)_2$, $2(NH_4)_2$ SO_4, $2H_2O$] (5.88×10^{-3} M) was used under acidic conditions (H_2SO_4, 9 N) in the presence of three drops of $Fe(o\text{-}phen)_3^{2+}$ as an indicator. To quantitatively determine the concentration of hydrogen peroxide, the H_2O_2 calibration curve was obtained by plotting the cerium volume (mL) as a function of H_2O_2 concentration (from 0 to 2.94×10^{-3} mol L^{-1}). The gradual change of the solution colour from red to the blue indicates a total oxidation of hydrogen peroxide using the cerium solution.

The ozone concentration was determined using the indigo method [35]. A stock solution of the indigo reagent was prepared by dissolving 770 mg L^{-1} of potassium indigo trisulphonate in 1 mL phosphoric acid. When the absorbance at 600 nm had decreased to below 80 % of the initial value, the stock solution of indigo was replaced (typically after 3–4 months storage). For low concentrations of ozone, 20 mL of indigo stock solution (2.49×10^{-5} M) was dissolved in 10 g monobasic sodium phosphate (Na_2HPO_4) and 7 mL phosphoric acid. The ozone calibration curve was obtained by plotting the absorbance as a function of O_3 concentration (standard solution with different concentrations from 0.0 to 1.87×10^{-6} moL L^{-1}). The standard solutions of ozone were prepared using an ozone generator (OzoStar, model WL7, Ozocan Corporation, Ontario, Canada).

3 Results and discussions

3.1 Characterisation of the Ti/TiO_2 electrode

The surface morphology of the TiO_2 photocatalytic coating was examined by scanning electron microscopy. Figure 2 shows a top view of a TiO_2 film deposited at 600 and 400 °C onto silicon substrates. The coating is densely featured with fine spherical grains of a few tens of diameters. By increasing the temperature from 400 to 600 °C, the deposited TiO_2 showed an increase in crystallite size. Figure 3a, b shows that the TiO_2 columns are densely packed with a uniform thickness across the film, forming a smooth and continuous interface with the underlying substrate. The crystallographic structure of the TiO_2 coating prepared by PLD was characterised by XRD (Fig. 4). The XRD analysis indicates that our TiO_2 coatings deposited at 600 and 400 °C are polycrystalline and crystallise in the TiO_2 rutile phase and in the TiO_2 anatase phase, respectively (Fig. 4a). The TiO_2 rutile phase is generally obtained for deposition at temperatures above 550 °C [36–38], while at temperature below 500 °C only the TiO_2 anatase phase is found [39]. The XRD spectrum of the TiO_2 coating on the Ti-grid confirms the presence of the same TiO_2 rutile phase and the same TiO_2 anatase phase obtained on Si (the peak intensities are less prominent than the peaks of the underlying metallic Ti-grid because of the thinness of the TiO_2 coating compared to the Ti-grid substrate) (Fig. 4b, c). Interestingly, one can note that the main (110) and (101) XRD peak of the TiO_2 phase is broader in the case of the films deposited onto the Ti-grid than on Si substrates. The average size of TiO_2 crystallites is smaller on the Ti-grid than on Si. To quantify this substrate-dependent grain size effect, the average size (D) of the TiO_2 crystallites was estimated using the Debye–Scherer equation [40]:

$$D = \frac{0.9\ \lambda}{\Delta(2\theta)\ \cos\theta} \tag{4}$$

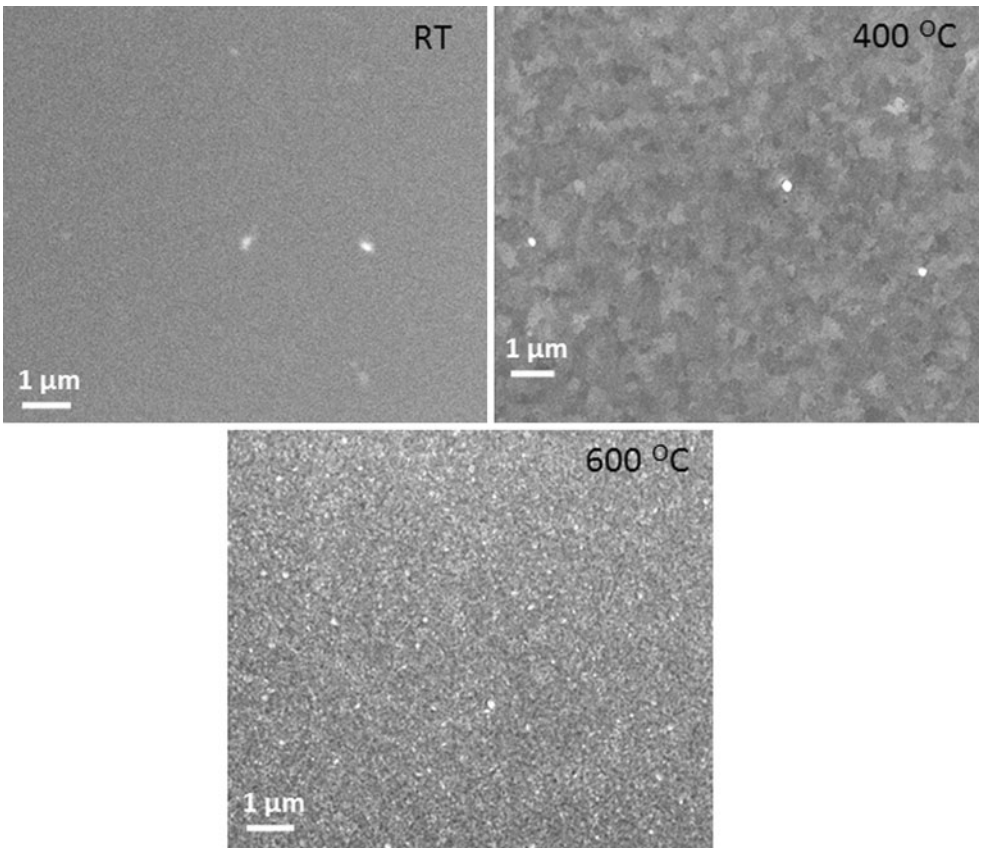

Fig. 2 SEM views of PLD TiO_2 films deposited on Si at different deposition temperatures

where D is the grain size in a particular orientation [i.e. (110) and (101) here], λ is the X-ray wavelength, 2θ is the diffraction angle corresponding to the particular orientation and $\Delta(2\theta)$ is the width at half maximum of the peak.

Thus, the average size of the TiO_2 rutile crystallites was estimated to be approximately 29 nm on silicon and only approximately 10 nm on the Ti-grid substrates. By comparison, the average size of the TiO_2 anatase crystallites was estimated to approximately 26 nm on silicon and only approximately 15 nm on the Ti-grid substrates. The smoothness of the silicon substrate promotes the growth of TiO_2 crystallites with increasing temperature.The average size of the TiO_2 particles (anatase) deposited on the Ti-grid is greater than the average size of TiO_2 rutile structure deposited on the Ti-gird. This result agrees with the data obtained from the SEM images and is likely due to the rougher surface of the Ti-grids compared to silicon grids. This nanometre scale grain size is expected to have an important effect on the photocatalytic activity of the TiO_2 coating [41]. Indeed, with a decrease in particle size, the catalytic activity is enhanced due to the huge increase in the surface area (or surface to volume ratio) of the material.

3.2 Bleaching of RNO

Experiments using direct photolysis (DP), electro-oxidation (EO), PC and PECO processes were carried out to compare the degradation efficiencies of RNO. The DP process involved exposing the RNO solution to UV irradiation at 254 nm, whereas in the PC process, UV light (254 nm) was used in the presence of the Ti/TiO_2 catalyst (rutile). The EO process was applied to the RNO solution using the Ti/TiO_2 catalyst at the anode, while in the PECO process the Ti/TiO_2 photoanode (rutile) was exposed to UV irradiation (254 nm) and an external potential. The results of RNO degradation using different experimental conditions are shown in Fig. 5. As is observed from this data, the bleaching rate of RNO increased with treatment time. The ROS were produced continuously over time and rapidly oxidised the nitroso groups. The RNO removal rate recorded in the solution over 120 min using the DP process was 6.52×10^{-3} mM h^{-1}. By comparison, exposure to the Ti/TiO_2 electrode (rutile) under UV irradiation (PC process) increases the degradation rate of RNO (6.69×10^{-3} mM h^{-1}). In the PC process, the photogeneration of oxidising species, such as hydroxyl radicals or holes, leads to their reaction with the conjugated

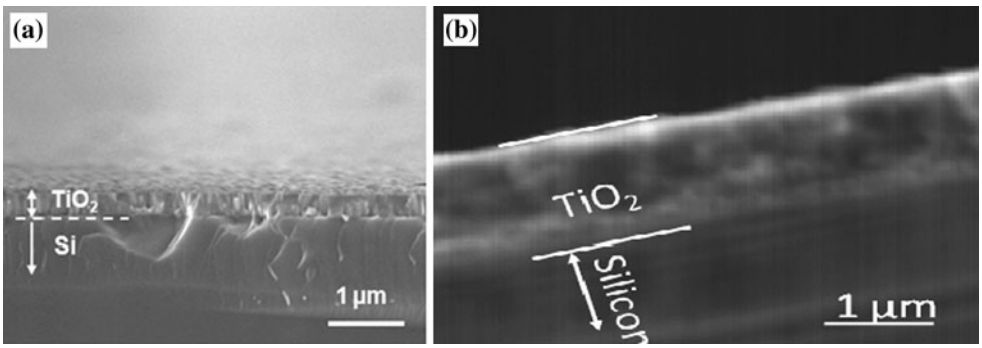

Fig. 3 SEM views of PLD TiO_2 films deposited on silicon

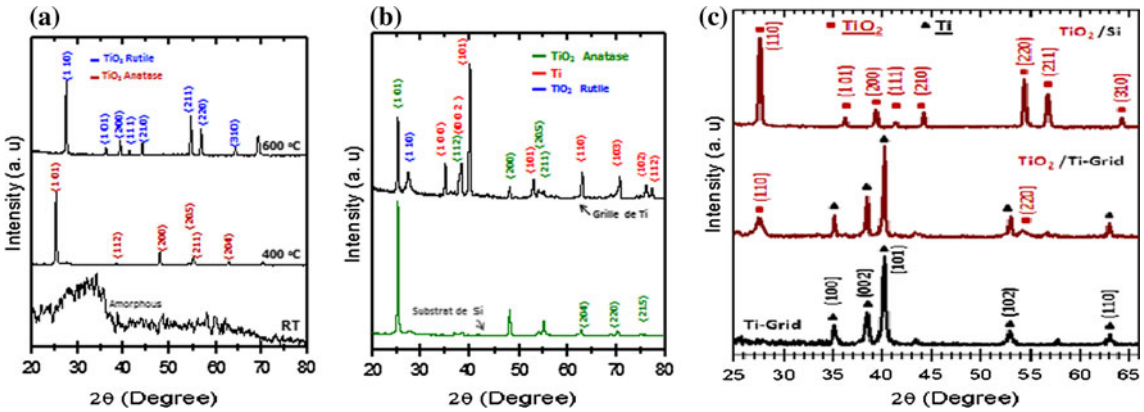

Fig. 4 X-ray diffraction patterns of TiO_2 film coated at **a** 600 and 400 °C; **b** on Si substrates and; **c** Ti-grids

double bonds in the π system of RNO and thus promotes the bleaching of RNO [23]. According to Zang et al. [32], the oxidation process is thermodynamically favoured because the VB of TiO_2 (+2.5 V/NHE at pH 7) is much higher than the oxidation potential of RNO (+0.3 V/NHE at pH 7). Furthermore, the degradation rate of RNO by the EO process was tested using rutile Ti/TiO_2 as an anode at 0.1 A. The removal rate of RNO recorded over 120 min of treatment was 7.12×10^{-3} mM h^{-1}. However, a more rapid RNO removal rate (15.9×10^{-3} mM h^{-1}) was recorded over 120 min using the PECO process with the Ti/TiO_2 photo-anode (rutile) at 0.1 A. In the PECO process, UV radiation activates the Ti/TiO_2 semi-conductor by ejecting an electron from the VB to the CB, while the applied external potential prevents recombination of the electron–hole pairs. These charge carriers (e^-/h^+) can migrate to the surface of the catalyst, where they are then available to undergo redox reactions with substrates [42]. The RNO bleaching rate was determined under DP, PC, EO and PECO conditions. The oxidising species (i.e. OH°, O_3, h^+) production rate is equal to the RNO disappearance rate according to Eq. (5)

$$r = \frac{\mathrm{d}[\mathrm{RNO}]}{\mathrm{d}t} = -k.[\mathrm{RNO}] \tag{5}$$

where '[RNO]' is the concentration of RNO, 'k' is the first-order reaction rate constant (t^{-1}) and 'r' is the production rate of oxidising species (such as OH°, h^+, O_3).

Integration of Eq. 5 gives:

$$\mathrm{Ln}\left(\frac{C_0}{C}\right) = k.t \tag{6}$$

where 'C_0' is the initial concentration of RNO, 'C' is the concentration of RNO at time t and 't' is the reaction time. The reaction rate constant 'k' could be calculated from the

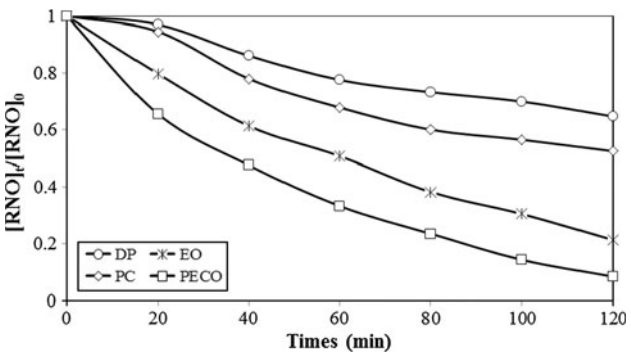

Fig. 5 Bleaching of RNO using different processes

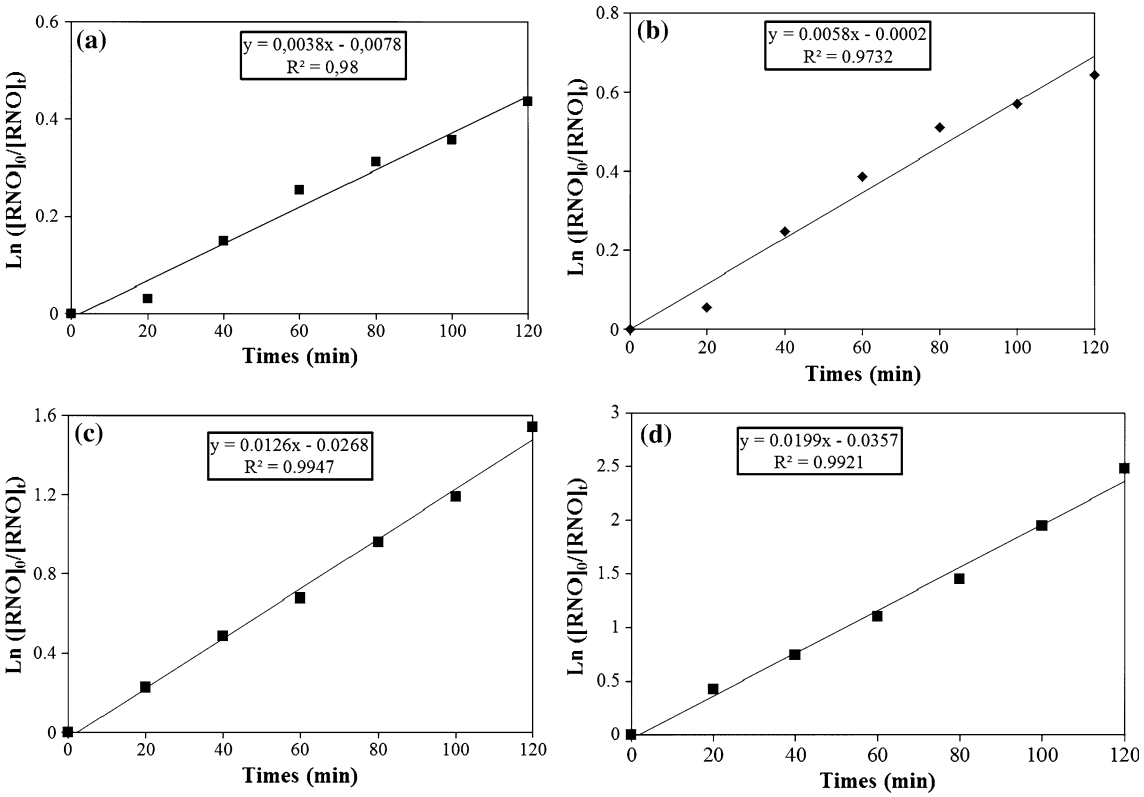

Fig. 6 Kinetic studies of bleaching of RNO using **a** DP, **b** PC, **c** EO and **d** PECO processes

slope of a plot of (t) versus Ln(C_0/C) from Eq. (6). Figure 6 shows that the RNO disappearance rate follows a first-order kinetic model. The first-order kinetic reaction rate constant in the PECO process was 0.02 min^{-1}. By comparison, the values of the apparent reaction rate constants for the DP, PC and EO processes were 0.0038, 0.0058 and 0.012 min^{-1}, respectively. The apparent reaction rate constant found for the PECO process was 3.4 times higher than that recorded under the PC conditions and 1.67 times higher than that measured using EO conditions. The contribution of external potential applied in photoelectrocatalytic process influences the production rate of oxidising species (OH°, h^+, O_3) and consequently the kinetic rate of pollutant degradation [43]. In the PECO process, the applied potential reduces the recombination rate of the photogenerated electron–hole pairs, enhances the production rate of oxidising species and consequently increases the bleaching rate of RNO. Therefore, the electrons and holes have more opportunities to participate in the degradation of RNO directly on the surface of nanostructured Ti/TiO_2 photo-anode (adsorption) or indirectly by reacting with oxidant species such as hydroxyl radicals [44]. RNO molecules were first adsorbed on Ti/TiO_2 and subsequently, the reactive oxygen species such as OH°, h^+ etc. predominantly attack the ring structure and induce the cleavage of the RNO. The mechanism of the adsorption of organic pollutant (such as rhodamine) on the photocatalyst surface (TiO_2 or TiO_2/SnO_2) using photocatalytic process has been widely highlighted by Chen et al. [45]. This work provide that the photocatalytic degradation of dye proceeds on the surface of the photocatalyst rather than on the bulk solution and the reactive oxygen species preferentially attack the molecular portion directly connected to the catalyst surface. However, the pollutant adsorbed on the surface of the catalyst can inhibit the reaction between the photo-generated holes (or hydroxyl radicals) and pollutant, and consequently decrease the degradation rate of pollutant [22]. A far as, the competition reaction between intermediate products for reacting with hydroxyl radicals could also inhibit the kinetic degradation of pollutant [18].

Several researchers [18, 22, 46] have shown that the efficiency of removing pollutants using the PECO process is influenced by various operating factors such as external potential, pH, UV light intensity and material phase structure. These parameters influence the oxidation potential, and consequently pollutant removal. Thus, the next step in our study was to investigate the effect of various operating parameters on the bleaching rate of RNO using the PECO process.

Table 1 Effect of crystallographic structure on the rate of RNO removal

Parameters	PECO process					
	Test 1	Test 2	Test 3	Test 4	Test 5	Test 6
Intensity (A)	0.1	0.1	0.1	0.05	0.05	0.05
Treatment times (min)	120	120	120	120	120	120
UV light intensity ($\mu W\ cm^{-2}$)	6,900	6,900	6,900	6,900	6,900	6,900
UV lamp position	Internal	Internal	Internal	Internal	Internal	Internal
Electrolyte (Na_2SO_4 M)	0.05	0.05	0.05	0.05	0.05	0.05
Type of cathode	Stainless steel	Stainless steel	Stainless steel	Stainless steel	Stainless steel	Stainless steel
Type of anode Structure (Ti/TiO_2)	Rutile	Anatase	Amorphous	Rutile	Anatase	Amorphous
Rate of RNO removal ($mM\ h^{-1}$)	0.12 ± 0.007	0.16 ± 0.02	0.10 ± 0.01	0.09 ± 0.007	0.12 ± 0.01	0.09 ± 0.015

PECO *photoelectrocatalytic oxidation*

3.3 Effect of the crystallographic structure

Three different structures of Ti/TiO_2 films (anatase, rutile, amorphous) were used for the PECO process to compare RNO removal efficiencies. The RNO removal rates using different experimental conditions (tests T1–T6) are shown in Table 1. For amorphous Ti/TiO_2, the RNO removal rate was slower than that recorded using anatase and rutile Ti/TiO_2 structures. The amorphous structure of Ti/TiO_2 contains large amounts of defects that can lead to an increase in the number of recombination sites for photo-generated electron–hole pairs, and consequently leads to a relatively low concentration of oxidising species [3, 47, 48]. The RNO degradation rate using the rutile structure was lower than that recording when using the anatase structure. RNO removal rates were 0.013 ± 0.0008 and 0.010 ± 0.0008 mMh^{-1} over 120 min using rutile Ti/TiO_2 at 0.1 and 0.05 A, respectively. In comparison, for the same current intensities (0.1 and 0.05 A), the average RNO removal rates using anatase Ti/TiO_2 were 0.018 ± 0.002 and 0.013 ± 0.001 $mM\ h^{-1}$, respectively. This result was not surprising because the band gap energy of the anatase phase (3.23 eV) is wider than that of the rutile phase (3.02 eV) [49]. This lower band gap energy of the rutile phase promotes the recombination of electrons and holes on the surface of the structure and reduces the production of oxidant species, such as hydroxyl radical. Thus, the anatase Ti/TiO_2 structure was selected for the next step of the experiments.

3.4 Effect of external potential

According to the literature [18, 19], external electrical potential is one of the key factors that improve photoelectrocatalytic efficiency. Applying an external potential at the TiO_2 photo-anode improves the separation of the photo-generated electrons and holes and prevents recombination.

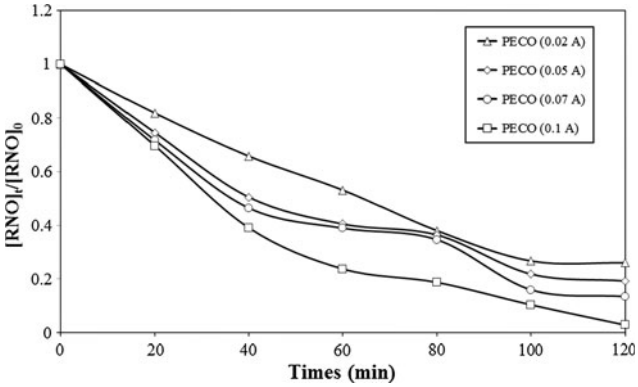

Fig. 7 Bleaching of RNO using the PECO process under different current intensities (effect of external potential) (at 254 nm and using Ti/TiO_2 anatase)

In our study, the effect of current intensity (from 0.02 to 0.1 A) was explored in the PECO process with irradiation at 254 nm using anatase Ti/TiO_2. Figure 7 shows the RNO degradation rate as a function of current intensity applied over the treatment time of 120 min. It can be observed that the RNO bleaching efficiency increased when the applied current increased from 0.02 to 0.1 A (from 7.2 to 13.1 V). The maximum RNO bleaching rate (17.3×10^{-3} $mM\ h^{-1}$) was obtained at 0.1 A over 120 min. In the PECO process, the electrical potential applied prevents the recombination of electron–hole pairs, increases the active hole lifetime and consequently increases the concentration of oxidant species, such as hydroxyl radicals [22, 50, 51]. The effect of electrical potential on hydroxyl radical production has been studied by Jiang et al. [2]. That study showed that the total concentration of hydroxyl radicals (higher than 20 $\mu mol\ L^{-1}$) generated under UV irradiation (20 W) was effectively enhanced with a small applied potential (0.6 V). Therefore, the current intensity selected for the next step of optimisation of the PECO process was 0.1 A.

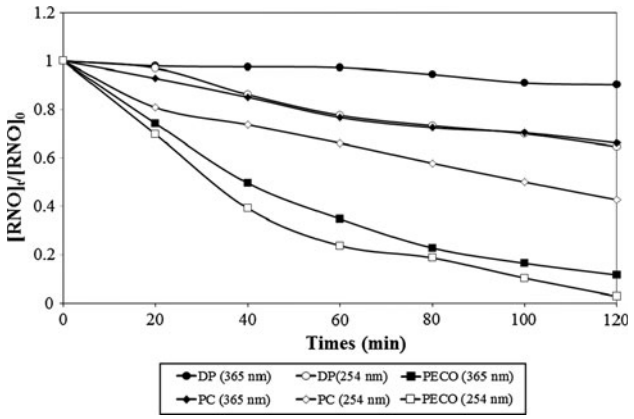

Fig. 8 Bleaching of RNO using the PECO process (at 0.1 A and using Ti/TiO_2 anatase) under different light intensities

3.5 Effect of light intensity

In the PC and PECO processes, the recombination of electron–hole pairs is a limiting step [52]. By increasing the intensity of the incident light, the probability of catalyst excitation and the re-excitation of recombined electrons are increased [18]. To assess the effect of light intensity (6,900 vs. 300 μW cm^{-2}) on the RNO bleaching rate, experiments using the DP, PC and PECO processes were carried out over 120 min of treatment time. The oxidative performance of the DP, PC and PECO processes (formation of active oxidant species) was evaluated by comparing the RNO bleaching rate under different light intensities. The results of RNO degradation using different experimental conditions are shown in Fig. 8. These results revealed that the bleaching rate increased with increasing the light intensity from 300 to 6,900 μW cm^{-2}. In the DP, PC and PECO processes, the removal rates of RNO recorded using a light intensity of 6,900 μW cm^{-2} (254 nm) were 6.52×10^{-3}, 8.55×10^{-3} and 17.3×10^{-3} mM h^{-1}, respectively. By comparison, the RNO removal rates detected using a light intensity of 300 μW cm^{-2} (365 nm) were 1.26×10^{-3} mM h^{-1} (DP), 5.36×10^{-3} mM h^{-1} (PC) and 15.7×10^{-3} mM (PECO). Thus, the decrease in the wavelength from 365 nm (0.3 mW cm^{-2}) to 254 nm (6.9 mW cm^{-2}) corresponds to an increase in the energy of the incident photon by a factor of 1.43 (according to the Planck equation $E = h\ c/\lambda$), whereas in terms of light intensity a factor of 23 is introduced. Thus, this higher degradation rate of RNO recorded by PECO process is mainly attributed to the effect of light intensity. The increase in the light intensity promotes the formation of reactive oxygen species (such as hydroxyl radicals) and improves the RNO bleaching rate. The effect of light intensity on the degradation of 4-chlorophenol using the photoelectrocatalytic process was also studied by Wang et al. [18]. Increasing light intensity (from 700 μW cm^{-2} to 2.5 mW cm^{-2}) enhances the formation of hydroxyl radicals and improves the degradation rate of 4-chlorophenol (95 % at 2.5 mW cm^{-2}). It has been proven by previous works [20] that the degradation rate of organic pollutant is proportional to the light intensity ($k^\circ = k_2\ I^b$, where k° is the degradation reaction rate; I is the light intensity and k_2 and b are the kinetic constants). As the photoelectrocatalytic bleaching rate of RNO was found to depend strongly on the applied light intensity applied to the surface of the catalysts, UV radiation with a light intensity of 6,900 μW cm^{-1} was selected for further study.

3.6 Effect of pH

In photocatalytic reactions, pH is one of the most important parameters that influence the degradation of pollutants [18, 53–55]. Solution pH affects the adsorption capacity and dissociation of the target compounds, the charge distribution of the photocatalyst surface, and the oxidation potential of the VB [18, 55, 56]. To investigate the effect of pH on the bleaching rate using the PECO process, the pH of the RNO solution was adjusted using 5 M NaOH or 1.5 M HCl. In a pH range of 6.2–10, the maximum RNO absorption peak is 440 nm, whereas at a pH value below 6.2, the maximum RNO absorption peak shifts to 350 nm [23, 33]. According to Simonsen et al. [23], the loss of the light absorption proprieties (from 440 to 350 nm) under acidic conditions is due to interaction of protons with the nitrogen atoms (in the tertiary amine or in the nitroso group) present in RNO molecule.

$$RNO_{(aq)} + H^+ \rightleftarrows RNOH^+_{(aq)} \quad (7)$$

The effect of pH on RNO degradation is shown in Fig. 9. With an increase in solution pH (from 2.7 to 11), the RNO bleaching rate (R_0) increased. The use of neutral and alkaline pH conditions was more beneficial to RNO bleaching. From the Fig. 9, we see that the highest bleaching rate (17.7×10^{-3} mM^{-1} h^{-1}) was recorded at a pH value of 7. For pH values above 7, the bleaching rate reaches a plateau. The changes in the RNO degradation rate with varying pH values can be attributed to variation of the acid/base properties of the TiO_2 surface [23]. When the pH is below 3.7, the TiO_2 surface becomes positively charged ($TiOH_2^+$) and strongly repels the RNO molecule, which can also possess a positive charge ($RNOH^+$). For pH values between 3.7 and 6.5, the bleaching rate was enhanced. In this range, there is a slight repulsion between the positively charged RNO molecule ($RNOH^+$) and the surface of TiO_2 (slightly charged) [32]. For pH values above 6.5, the electrostatic attraction between the negatively charged TiO_2 surface (TiO^-) and the RNO molecule was enhanced, and the bleaching rate increased. The results recorded in our study are consistent with the results

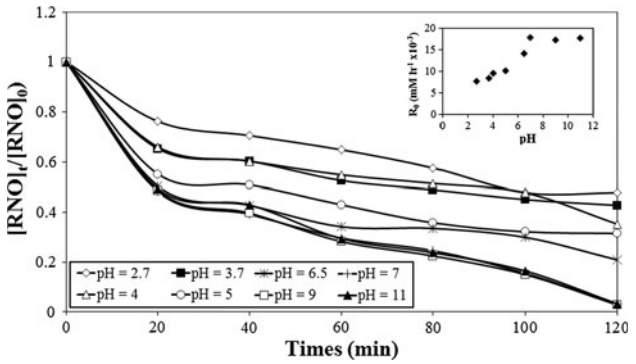

Fig. 9 Bleaching of RNO using the PECO process (at 0.1 A under 254 nm using Ti/TiO_2 anatase) at different pH

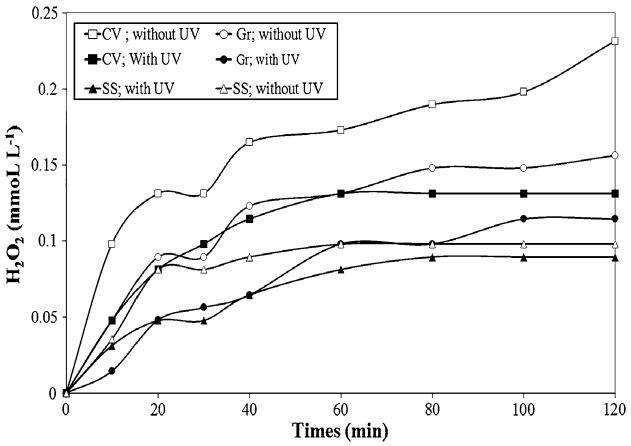

Fig. 10 H_2O_2 production during electrolysis at 0.1 A and under 254 nm

obtained by Zang et al. [32] who studied the effect of pH on RNO bleaching using the PC process. These results demonstrate clearly that a pH value of 7.0 is optimal for effective RNO bleaching. According to previous research work [57, 58], the adsorption of organic molecules on the surface of photocatalysts had been proved to influence greatly the photocatalytic degradation of the organic compounds. For instance, TiO_2 and TiO_2/SnO_2 systems were investigated by Chen et al. [45] to understand the influence of the adsorption mode and illumination radiation in the degradation of rhodamine B. The adsorption of rhodamine B on the TiO_2/SiO_2 surface has been recorded by the positively charged diethylamino group while in the case of TiO_2, it adsorbs through the negatively charged carboxyl group [45]. Subsequently, the reactive oxygen species produced by photocatalytic process ensure the degradation of rhodamine.

3.7 Effect of H_2O_2 produced at the cathode electrode

The main objective is to evaluate the effect of ROS produced in situ on the RNO bleaching efficiency. ROS, such as H_2O_2, can be generated at the cathode [25]. The addition of oxidising species, such as H_2O_2 is beneficial for photocatalytic reaction by trapping the electron in the CB and generating more hydroxyl radicals [25, 26].

Three types of cathode electrodes (SS, Gr and VC) were tested to evaluate their capacity for H_2O_2 production in the photoelectrocatalytic cell using a solution of distilled water and Na_2SO_4 (0.05 M) without the addition of RNO. Experiments were performed using Ti/TiO_2 (anatase) as the photo-anode with (or without) UV irradiation (254 nm). Hydrogen peroxide concentrations generated under the different experimental conditions are shown in Fig. 10. The maximum concentration of H_2O_2 (0.23 mM) was recorded after a treatment time of 120 min using VC as the cathode at a current intensity of 0.1 A without UV illumination. Under the same conditions, the concentration of H_2O_2 detected after 120 min using Gr as the cathode was 0.15 mM. Recent studies have demonstrated that VC and Gr used as a cathode material can lead to the electrochemical generation of H_2O_2 [25]. However, it was surprising to measure a residual H_2O_2 concentration in solution using SS as a cathode material.

In fact, the H_2O_2 ($\sim$0.09 mM) produced during 120 min of electrolysis was not produced at the SS cathode, but it was produced on the photo-anode material. The same trend has been also obtained by Daghrir et al. [59] while studying the photoelectrocatalytic oxidation of CTC using different cathode materials. The residual H_2O_2 concentration recorded at 0.39 A of current intensity, after 120 min of treatment time and using Ti/TiO_2 (anatase) as anode and SS as cathode was 0.09 $\pm$ 0.002 mM. The observed peroxide was mainly formed during reactions [Eqs. (8)–(14)] occurring at the surface of the Ti/TiO_2 catalyst [59, 60]. H_2O_2 is one of the oxidising species that can be formed on the surface of Ti/TiO_2 in the presence or in the absence of UV irradiation. Indeed, in the absence of UV irradiation, only the applied current (or the potential difference) during electrolysis results in excitation of the Ti/TiO_2 catalyst. Under these conditions, adsorbed oxygen [$O_{2(ads)}$] can directly participate in the reaction by trapping the electron (e^-) present in the CB, generating superoxide anion ($O_2^{\circ -}$), and subsequently H_2O_2. The reduction mechanism of O_2 to generate $O_2^{\circ -}$ is thermodynamic favoured as the conduction band of TiO_2 (−0.52 V) is much electronegative than reduction potential of $O_2/O_2^{\circ -}$ (−0.33 V) [61].

$$e^- + O_{2(ads)} \rightarrow O_2^{\circ -} \quad (8)$$

$$O_2^{\circ -} + H^+ \rightarrow HO_2^{\circ} \quad (9)$$

$$2HO_2^{\circ} \rightarrow H_2O_2 + O_2 \quad (10)$$

$$O_2^{\circ -} + HO_2^{\circ} \rightarrow O_2 + HO_2^- \quad (11)$$

$$HO_2^- + H^+ \rightarrow H_2O_2 \quad (12)$$

$$O_2 + 2e_{CB} + 2H^+ \rightarrow H_2O_2 \quad (13)$$

$$2H_2O + 2h^+_{VB} \rightarrow H_2O_2 + 2H^+_{aq} \quad (14)$$

Nevertheless, under UV irradiation (254 nm), H_2O_2 concentrations recorded after 120 min of treatment at a current intensity of 0.1 A using VC, Gr and SS as the cathode were 0.15, 0.11 and 0.07 mM, respectively. The decrease in the concentration of H_2O_2 was attributed to hydroxyl radical formation, which is generated from the decomposition of H_2O_2 under UV irradiation [Eq. (15)] [5, 62, 63].

$$H_2O_2 + h\upsilon \rightarrow 2OH^\circ \quad (15)$$

To evaluate the effect of the cathode on the RNO bleaching rate, additional experiments were carried out using the following conditions: 0.1 A under, UV irradiation at 254 nm, 4.80×10^{-5} M RNO. The different cathode electrode materials (SS, Gr, and VC) were explored. The bleaching rate recorded using VC as a cathode material was 22.6×10^{-3} mM h^{-1}. By comparison, the RNO bleaching rates recorded using SS and Gr as cathode electrodes were 15.8×10^{-3} and 19.2×10^{-3} mM h^{-1}, respectively. The significantly higher rate (22.6×10^{-3} mM h^{-1}) of RNO bleaching recorded using VC as cathode and TiO_2 (anatase form) as photoanode is mainly due the oxidising species (OH°, h^+, O_3) generated by PECO process. Besides, the bleaching rate of RNO may be due to the reductive mechanism. The reduction potential of RNO has been reported to be +0.04 V versus NHE at pH 7.0, which is more electropositive than the conduction band of TiO_2 (−0.52 V) [32]. Thus, the photo-generated electrons on the conduction band are able to reduce RNO. The reduction process is believed to bring an electron into the antibonding π electron system of RNO promoting the decrease of the total bonding energy of the π electron system and cleave the bond [23]. It could be interesting to compare the bleaching rate of RNO recorded by PECO process with those obtained in others experimental conditions. Simonsen et al. [23] indicated that the photocatalytic bleaching rate of RNO using TiO_2 coated liner under UV irradiation (14 W low pressure lamp, 254 nm, 20 mW cm^{-2}) is 8.9×10^{-9} M s^{-1}. This bleaching rate reported in the literature is higher than those recorded in the present study. The corresponding bleaching rate recorded by PECO process in our study (62×10^{-10} M s^{-1}) was lower than that recorded by Simonsen et al. [23]. The contribution of experimental conditions such as the light intensity influences the production rate of oxidising species (h^+, OH°, etc.) and consequently the bleaching rate of RNO. The UV light intensity imposed during the photoelectrocatalytic process (6.9 mW cm^{-2}) was lower than the UV light imposed by Simonsen et al. [23].

3.8 Effect of ozone production

Ozone is a very strong oxidant ($E^\circ = 1.51$ V/ENH) that can be generated by electrolytic oxidation of a water molecule (Eq. 16) [64]. The capacity for ozone production in the photoelectrocatalytic cell under the typical synthetic conditions [distilled water + Na_2SO_4 (0.05 M) without RNO addition] was evaluated. The final concentration of ozone recorded after 120 min of electrolysis at 0.1 A using Ti/TiO_2 (anatase) as the photo-anode and VC as the cathode with UV irradiation (254 nm) was approximately 0.313 μM. Ozone generated in situ can directly participate in the bleaching of RNO [23]. However, when the photocatalytic reaction was initiated (under UV radiation), hydroxyl radicals were generated from the decomposition of ozone [Eqs. (17)–(19)] [65]. The decomposition of ROS (such as H_2O_2 and O_3) increases the hydroxyl radical concentration and leads to an enhanced RNO bleaching rate.

$$3\,H_2O \rightarrow O_3 + 6\,H^+ + 6e^- \quad (16)$$

$$O_3 + h\upsilon \rightarrow O_2 + O^o \quad (17)$$

$$O^o + H_2O \rightarrow 2OH^o \quad (18)$$

$$O_3 + OH^o \rightarrow HO_2^o + O_2 \quad (19)$$

4 Conclusion

In this study, a rectangular Ti/TiO_2 electrode was prepared by a PLD method. The TiO_2 coating formed at 600 and 400 °C is very uniform in thickness and forms a continuous interface with the substrate. In addition, X-ray diffraction analysis indicated that the TiO_2 coating formed on the Ti-grid is of the rutile phase and the coating formed on Si is of the anatase phase. The main (110) and (101) XRD peaks of the rutile and anatase structures are broader in the case of TiO_2 deposited onto the Ti-grid than on the Si substrate. Using Ti/TiO_2 nanostructured electrodes, a photoelectrocatalytic cell was constructed and evaluated in terms of its capacity to degrade RNO. The current intensity, crystallographic structure of the Ti/TiO_2 anode, type of cathode material, UV irradiation and initial pH all had a significant influence on the RNO bleaching rate. The photoelectrocatalytic cell prepared using anatase Ti/TiO_2 as the photoanode and VC as the cathode electrode, operated at a current of 0.1 A for 120 min with UV irradiation (254 nm), was found to be the best for removing large amounts of RNO at a rate of 22.63×10^{-3} mM h^{-1}. However, the identification of by-products needs to be rigorously verified and a mechanism of RNO degradation should be proposed. The photoelectrocatalytic technique could form the basis of a process capable of removing refractory organic

compounds from many natural and wastewater sources (drinking water, industrial and municipal wastewater). The next step of this study should be the treatment of water contaminated by emerging and persistent organic pollutants (POPs), such as antibiotics, pesticides, oestrogenic compounds and alkylphenols, using a surface response methodology.

Acknowledgments Sincere thanks are extended to the National Sciences, Engineering Research Council of Canada and Premier Tech Ltée for their financial support of this study.

References

1. Hoffmann MR, Martin ST, Choi W, Bahnemann DW (1995) Environmental applications of semiconductor photocatalysis. Chem Rev 95(1):69–96
2. Jiang YL, Liu HL, Wang QH, Jiang ZH (2006) Determination of hydroxyl radicals in TiO_2/Ti photoelectrocatalytic oxidation system using $Fe(phen)_3^{2+}$ spectrophotometry. J Environ Sci 18(1):158–161
3. Xiang Q, Yu J, Wong PK (2011) Quantitative characterization of hydroxyl radicals produced by various photocatalysts. J Colloid Interface Sci 357(1):163–167
4. Li XZ, Liu HL, Yue PT, Sun YP (2000) Photoelectrocatalytic oxidation of rose Bengal in aqueous solution using a Ti/TiO_2 mesh electrode. Environ Sci Technol 34(20):4401–4406
5. Ollis DF, Pelizzetti E, Serpone N (1991) Photocatalysed destruction of water contaminants. Environ Sci Technol 25(9): 1522–1529
6. Hidaka H, Nohara K, Zhao J, Serpone N, Pelizzetti E (1992) Photo-oxidative degradation of the pesticide permethrin catalyzed by irradiated TiO_2 semiconductor slurries in aqueous media. J Photochem Photobiol A 64(2):247–254
7. Li J, Li LJ, Zheng L, Xian Y, Jin L (2006) Photoelectrocatalytic degradation of rhodamine B using Ti/TiO_2 electrode prepared by laser calcination method. Electrochim Acta 51(23):4942–4949
8. Reyes C, Fernandez J, Freer J, Mondaca MA, Zaror C, Malato S, Mansilla H (2006) Degradation and inactivation of tetracycline by TiO_2 photocatalysis. J Photochem Photobiol A 184:141–146
9. Fukahori S, Ichiura H, Kitaoka T, Tanaka H (2003) Photocatalytic decomposition of bisphenol A in water using composite TiO2–Zeolite sheets prepared by a papermaking technique. Environ Sci Technol 37:1048–1051
10. Kaniou S, Pitarakis K, Barlagianni I, Poulios I (2005) Photocatalytic oxidation of sulfamethazine. Chemosphere 60:372–380
11. Waldner G, Pourmodjib M, Bauer R, Neumann-Spallart M (2003) Photoelectrocatalytic degradation of 4-chlorophenol oxalic acid on titanium dioxide electrodes. Chemosphere 50(8):989–998
12. Daghrir R, Drogui P, Didier R (2012) Photoelectrocatalytic technologies for environmental applications. J Photochem Photobiol A Chem 238:41–52
13. Meng F, Hong Z, Arndt J, Li M, Zhi M, Yang F, Wu N (2012) Visible light photocatalytic activity of nitrogen-doped $La_2Ti_2O_7$ nanosheets originating from band gap narrowing. Nano Res 5(3):213–221
14. Cushing SK, Li J, Meng F, Senty TR, Suri S, Zhi M, Li M, Bristow AD, Wu N (2012) Photocatalytic activity enhanced by plasmonic resonant energy transfer from metal to semiconductor. J Am Chem Soc 134(36):15033–15041
15. Ma TY, Yuan ZY, Cao JL (2010) Hydrangea-like meso-/macroporous ZnO–CeO_2 binary oxide materials: synthesis, photocatalysis and CO oxidation. Eur J Inorg Chem 2010(5):716–724
16. Teh CM, Mohamed AR (2011) Role of titanium dioxide and ion-doped titanium dioxide on photocatalytic degradation of organic pollutants (phenol compounds and dyes) in aqueous solutions: a review. J Alloys Compd 509:1648–1660
17. Burda C, Lou Y, Chen X, Samia ACS, Stout J, Gole JL (2003) Enhanced nitrogen doping in TiO_2 nanoparticles. Nano Lett 3: 1049–1051
18. Wang N, Li X, Wang Y, Quan X, Chen G (2009) Evaluation of bias potential enhanced photocatalytic degradation of 4-chlorophenol with TiO_2 nanotube fabricated by anodic oxidation method. Chem Eng J 146(1):30–35
19. Selcuk H, Sene JJ, Anderson MA (2003) Photoelectrocatalytic humic acid degradation kinetics and effect of pH, applied potential and inorganic ions. J Chem Technol Biotechnol 78(9): 979–984
20. Li XZ, Li FB, Fan CM, Sun YP (2002) Photoelectrocatalytic degradation of humic acid in aqueous solution using a Ti/TiO_2 mesh photoelectrode. Water Res 36(9):2215–2224
21. Fujishima A, Rao TN, Tryk AD (2000) Titanium dioxide photocatalysis. J Photochem Photobiol C 1:1–21
22. Ding Y, Yang C, Zhu L, Zhang J (2010) Photoelectrochemical activity of liquid phase deposited TiO_2 film for degradation of benzotriazole. J Hazard Mater 175:96–103
23. Simonsen ME, Muff J, Bennedsen LR, Kowalski KP, SØgaard EG (2010) Photocatalytic bleaching of *p*-nitrosodimethylaniline and a comparison to the performance of other AOP technologies. J Photochem Photobiol A 216:244–249
24. Ozer RR, Ferry JL (2001) Investigation of the photocatalytic activity of TiO_2-polyoxometalate systems. Environ Sci Technol 35(15):3242–3246
25. Xie YB, Li XZ (2006) Degradation of bisphenol A in aqueous solution by H_2O_2 assisted photoelectrocatalytic oxidation. J Hazard Mater B138:526–533
26. Sohrabi MR, Ghavami M (2010) Comparison of direct yellow 12 dye degradation efficiency using UV/semiconductor and UV/H_2O_2/semiconductor systems. Desalination 252(1–3):157–162
27. Ishibashi Ki, Fujishima A, Watanabe T, Hashimoto K (2000) Detection of active oxidative species in TiO_2 photocatalysis using the fluorescence technique. Electrochem Commun 2(3):207–210
28. Halpern HJ, Yu C, Barth E, Peric M, Rosen GM (1995) In situ detection, by spin trapping, of hydroxyl radical markers produced from ionizing radiation in the tumor of a living mouse. Proc Natl Acad Sci USA 92(3):796–800
29. Ishibashi Ki, Fujishima A, Watanabe T, Hashimoto K (2000) Quantum yields of active oxidative species formed on TiO_2 photocatalyst. J Photochem Photobiol A 134(1–2):139–142
30. Jen JF, Leu MF, Yang TC (1998) Determination of hydroxyl radicals in an advanced oxidation process with salicylic acid trapping and liquid chromatography. J Chromatogr A 796(2): 283–288
31. Kraljié I, Trumbore CN (1965) *p*-Nitrosodimethylaniline as an OH radical scavenger in radiation chemistry. J Am Chem Soc 87:2547–2550
32. Zang L, Qu P, Zhao J, Shen T, Hidaka H (1997) Photocatalytic bleaching of *p*-nitrosodimethylaniline in TiO_2 aqueous suspensions: a kinetic treatment involving some primary events photo-induced on the particle surface. J Mol Catal A Chem 120(1–3): 235–245
33. Muff J, Bennedsen LR, SØgaard EG (2011) Study of electrochemical bleaching of *p*-nitrosodimethylaniline and its role hydroxyl radical probe compound. J Appl Electrochem 41(5): 599–607
34. Desbiens E, El Khakani MA (2003) Growth of high-K silicon oxynitride thin films by means of a pulsed laser deposition-atomic nitrogen plasma source hybrid system for gate dielectric applications. J Appl Phys 94(9):5969–5975

35. Bader H, Hoigné J (1981) Determination of ozone in water by the indigo method. Water Res 15(4):449–456
36. Kitazawa Si, Choi Y, Yamamoto Sh, Yamaki T (2006) Rutile and anatase mixed crystal TiO_2 thin films prepared by pulsed laser deposition. Thin Solid Films 515(4):1901–1904
37. Jaroenworaluck A, Regonini D, Bowen CR, Stevens R (2010) A microscopy study of the effect of heat treatment on the structure and properties of anodized TiO_2 nanotubes. Appl Surf Sci 256: 2672–2679
38. Regonini D, Jaroenworaluck A, Stevens R, Bowen CR (2010) Effect of heat treatment on the properties and structure of TiO_2 nanotubes: phase composition and chemical composition. Surf Interface Anal 42:139–144
39. Fang D, Luo Z, Huang K, Lagoudas DC (2011) Effect of heat treatment on morphology, crystalline structure and photocatalysis properties of TiO_2 nanotubes on Ti substrate and freestanding membrane. Appl Surf Sci 257(15):6451–6461
40. Guinier A (1962) Théorie et Technique de la radiocristallographie, 3rd edn. Dunod, Paris
41. Kim CS, Kwon IM, Moon BK, Jeong JH, Choi BC, Kim JH, Choi H, Yi SS, Yoo DH, Hong KS, Park JH, Lee HS (2007) Synthesis and particle size effect on the phase transformation of nanocrystalline TiO_2. Mater Sci Eng C 27:1343–1346
42. Yang J, Dai J, Chen C, Zhao J (2009) Effects of hydroxyl radicals and oxygen species on the 4-chlorophenol degradation by photoelectrocatalytic reactions with TiO_2-film electrodes. J Photochem Photobiol A Chem 208:66–77
43. Daghrir R, Drogui P, Ka I, El-Khakani MA (2012) Photoelectrocatalytic degradation of chlortetracycline using Ti/TiO_2 nanostructured electrodes deposited by means of a pulsed laser deposition process. J Hazard Mater 199–200:15–24
44. Adams C, Wang MY, Loftin K, Meyer M (2002) Removal of antibiotics from surface and distilled water in conventional water treatment processes. J Environ Eng 128:253–260
45. Chen F, Zhao J, Hidaka H (2003) Highly selective deethylation of rhodamine B: adsorption and photooxidation pathways of the dye on the TiO_2/SiO_2 composite photocatalyst. Int J Photoenergy 5(4):209–217
46. Leng WH, Zhu WC, Ni J, Zhang Z, Zhang JQ, Cao CN (2006) Photoelectrocatalytic destruction of organics using TiO_2 as photoanode with simultaneous production of H_2O_2 at the cathode. Appl Catal A 300(1):24–35
47. Yu J, Zhang L, Cheng B, Su Y (2007) Hydrothermal preparation and photocatalytic activity of hierarchically sponge-like macro-/mesoporous Titania. J Phys Chem C 111:10582–10589
48. Yu J, Wang G, Cheng B, Zhou M (2007) Effects of hydrothermal temperature and time on the photocatalytic activity and microstructures of bimodal mesoporous TiO_2 powders. Appl Catal B 69(3–4):171–180
49. Yoon KH, Noha JS, Kwon CH, Muhammed M (2006) Photocatalytic behavior of TiO_2 thin films prepared by sol–gel process. Mater Chem Phys 95(1):79–83
50. An T, Zhang W, Li G, Xiao X, Sheng G, Fu J, Zhu X (2004) Photoelectrocatalytic degradation of quinolone with a novel three-dimensional electrode-packed bed photocatalytic reactor. J Photochem Photobiol A 161:233–242
51. Vinodgopal K, Hotchandani S, Kamat PV (1993) Electrochemically assisted photocatalysis TiO_2 particulate film electrodes for photocatalytic degradation of 4-chlorophenol. J Phys Chem 97:9040–9044
52. Venkatachalam N, Palanichamy M, Arabindoo B, Murugesan V (2007) Enhanced photocatalytic degradation of 4-chlorophenol by Zr^{4+} doped nano TiO_2. J Mol Catal A Chem 266(1–2): 158–165
53. Liang HC, Li XZ, Yang YH, Sze KH (2008) Effects of dissolved oxygen, pH, and anions on the 2,3-dichlorophenol degradation by photocatalytic reaction with anodic TiO_2 nanotube films. Chemosphere 73(5):805–812
54. Gaya UI, Abdullah AH (2008) Heterogeneous photocatalytic degradation of organic contaminants over titanium dioxide: a review of fundamentals, progress and problems. J Photochem Photobiol C 9(1):1–12
55. Quan X, Ruan X, Zhao H, Chen S, Zhao Y (2007) Photoelectrocatalytic degradation of pentachlorophenol in aqueous solution using a TiO_2 nanotube film electrode. Environ Pollut 147(2): 409–414
56. Chong MN, Jin B, Chow CWK, Saint C (2010) Recent developments in photocatalytic water treatment technology: a review. Water Res 44(10):2997–3027
57. Xu Y, Langford CH (2001) UV- or visible-light-induced degradation of X3B on TiO_2 nanoparticles: the influence of adsorption. Langmuir 17:897–902
58. Zhao J, Wu T, Wu K, Okikawa K, Hidaka H, Serpone N (1998) Photoassisted degradation of dye pollutants. 3. Degradation of the cationic dye rhodamine B in aqueous anionic surfactant/TiO_2 dispersions under visible light irradiation: evidence for the need of substrate adsorption on TiO_2 particles. Environ Sci Technol 32:2394–2400
59. Daghrir R, Drogui P, El-Khakani MA (2013) Photoelectrocatalytic degradation of chlortetracycline using Ti/TiO_2 photo-anode with simultaneous H_2O_2 production. Electrochem Acta 87:18–31
60. Macphee DE, Rosenberg D, Skellern MG, Wells RP, Duffy JA, Killham KS (2011) A tungsten oxide-based photoelectrocatalyst for degradation of environmental contaminants. J Solid State Electrochem 15(1):99–103
61. Wood PM (1998) The potential diagram for oxygen at pH 7. Biochem J 253:287–289
62. Hua Z, Manping Z, Zongfeng X, Low GKC (1995) Titanium dioxide mediated photocatalytic degradation of monocrotophos. Water Res 29(12):2681–2688
63. Tizaoui C, Mezughi K, Bickley R (2011) Heterogeneous photocatalytic removal of the herbicide clopyralid and its comparison with UV/H_2O_2 and ozone oxidation techniques. Desalination 273(1):197–204
64. Kitsuka K, Kaneda K, Ikematsu M, Iseki M, Mushiake K, Ohsaka T (2009) Ex situ and in situ characterization studies of spin-coated TiO_2 film electrodes for the electrochemical ozone production process. Electrochim Acta 55(1):31–36
65. Hong Q, De-zhi S, Guo-qing C (2007) Formaldehyde degradation by UV/TiO_2/O_3 process using continuous flow mode. J Environ Sci 19:1136–1140